



Spatio-temporal modelling of changes in air pollution exposure associated to the COVID-19 lockdown measures across Europe



Anton Beloconi, Nicole M. Probst-Hensch, Penelope Vounatsou*

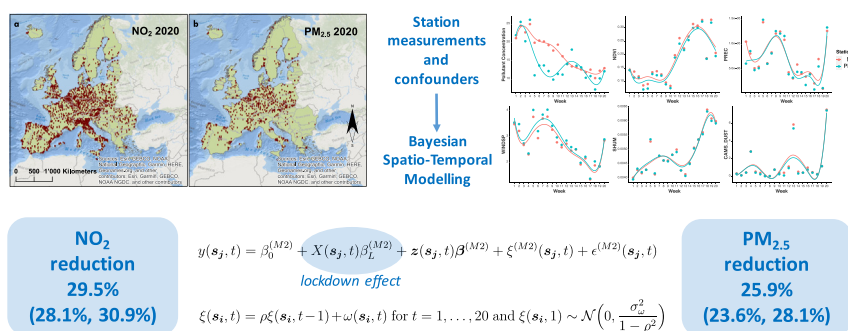
^a Swiss Tropical and Public Health Institute, Basel, Switzerland

^b University of Basel, Switzerland

HIGHLIGHTS

- The effect of COVID-19 lockdown on air pollution exposure in Europe was estimated.
- Bayesian space-time models were fitted adjusting for seasonality and confounders.
- Actual lockdown effect cannot be estimated without considering contextual factors.
- Lockdown-related reduction of NO₂ and PM_{2.5} was 30% and 26%, respectively.
- Targeted governmental policies can considerably reduce air pollution in short time.

GRAPHICAL ABSTRACT



ARTICLE INFO

Article history:

Received 23 February 2021

Received in revised form 3 May 2021

Accepted 5 May 2021

Available online 11 May 2021

Editor: Jianmin Chen

Keywords:

PM_{2.5}

NO₂

Gaussian processes

Bayesian inference

Air quality policy evaluation

Copernicus

ABSTRACT

The lockdown and related measures implemented by many European countries to stop the spread of the SARS-CoV-2 virus (COVID-19) pandemic have altered the economic activities and road transport in many cities. To rigorously evaluate how these measures have affected air quality in Europe, we developed Bayesian spatio-temporal (BST) models that assess changes in the surface nitrogen dioxide (NO₂) and fine particulate matter (PM_{2.5}) concentration across the continent. We fitted BST models to measurements of the two pollutants in 2020 using a lockdown indicator covariate, while accounting for the spatial and temporal correlation present in the data. Since other factors, such as weather conditions, local combustion sources and/or land surface characteristics may contribute to the variation of pollutant concentrations, we proposed two model formulations that allowed the differentiation between the variations in pollutant concentrations due to seasonality from the variations associated to the lockdown policies. The first model compares the changes in 2020, with the ones during the same period in the previous five years, by introducing an offset term, which controls for the long-term average concentrations of each pollutant during 2014–2019. The second approach models only the 2020 data, but adjusts for confounding factors. The results indicated that the latter can better capture the lockdown effect. The measures taken to tackle the virus in Europe reduced the average surface concentrations of NO₂ and PM_{2.5} by 29.5% (95% Bayesian credible interval: 28.1%, 30.9%) and 25.9% (23.6%, 28.1%), respectively. To our knowledge, this research is the first to account for the spatio-temporal correlation present in the monitoring data during the pandemic and to assess how it affects estimation of the lockdown effect while accounting for confounding. The proposed methodology improves our understanding of the effect of COVID-19 lockdown policies on the air pollution burden across the continent.

© 2021 The Authors. Published by Elsevier B.V. This is an open access article under the CC BY-NC-ND license (<http://creativecommons.org/licenses/by-nc-nd/4.0/>).

* Corresponding author at: Swiss Tropical and Public Health Institute, Basel, Switzerland.

E-mail addresses: anton.beloconi@swisstph.ch (A. Beloconi), nicole.probst@swisstph.ch (N.M. Probst-Hensch), penelope.vounatsou@swisstph.ch (P. Vounatsou).

1. Introduction

The unique situation created by the SARS-CoV-2 virus pandemic (COVID-19) has led to a sudden decrease in economic activities (OECD, 2020). The governments' restrictions aimed to tackle the spread of the virus, such as the stay-at-home policies and closed international borders, significantly reduced the traffic volume (Apple, 2020; Brunekreef et al., 2021). Emerging evidence suggests that these changes resulted in noticeable reductions of pollutant concentrations in ambient air (Shakil et al., 2020). Particularly, the concentration of nitrogen dioxide (NO_2) has dropped in many cities around the world (Ogen, 2020; Zhang et al., 2020), while changes in fine particulate matter ($PM_{2.5}$) have been more limited and less consistent (Dantas et al., 2020; Menut et al., 2020; Putaud et al., 2020; Sharma et al., 2020).

Ground-level NO_2 and $PM_{2.5}$ concentrations continue to represent a serious public health concern in Europe. In recent years, about 16 million Europeans were exposed to NO_2 levels above those proposed by the WHO air quality guidelines (Beloconi and Vounatsou, 2020), while around 350 million people across the continent were exposed to elevated $PM_{2.5}$ levels (Beloconi et al., 2018). Exposure to air pollution contributes to the development of diabetes, high blood pressure, heart and lung diseases (Cohen et al., 2017), decreases immunity (Mostafavi et al., 2019) and induces inflammation (Chen and Schwartz, 2008). Recent COVID-19 studies suggest that individuals with such underlying comorbidities may be more susceptible to the impact of the coronavirus infection and at higher risk of mortality from COVID-19 (Wang et al., 2020; Yang et al., 2020). Therefore, estimates of the changes in air quality caused by the measures implemented to tackle the spread of the virus are very necessary. They would help quantifying a potential reduction in morbidity associated with air pollution exposure during the lockdown and to improve our understanding of the impact of related policies on air pollution burden.

Although a large number of literature reports changes in air pollution levels that occurred during and after the COVID-19 lockdown measures, very few efforts have rigorously modelled the effect of the lockdown while accounting for confounding factors, e.g. variation due to natural weather conditions or other spatio-temporal characteristics, such as seasonality. A representative sample of the literature is provided in Table A1 (in the appendix). The majority of the articles have used explorative analyses, such as graphical comparisons between average pollutant concentration levels during the lockdown periods in 2020 and similar periods in previous years, or between pre- and post- "intervention" periods (e.g. Abdullah et al., 2020; Dantas et al., 2020). The data sources used to illustrate the differences in the pollutant concentrations were mostly based on ground-level air quality measurements from monitoring stations, satellite-derived tropospheric measurements, air pollutant simulations obtained from chemical transport models (CTMs), or combination of these sources (e.g. Barré et al., 2020; Goldberg et al., 2020). Several works have used pairwise t-test to evaluate the statistical significance of these differences (e.g. Dobson and Semple, 2020; Giani et al., 2020; Putaud et al., 2020).

Since many parameters, including local combustion sources, land surface characteristics, atmospheric and weather conditions influence NO_2 and $PM_{2.5}$ formation and dispersion (Chudnovsky et al., 2014; Bechle et al., 2015; Stafoggia et al., 2017; Young et al., 2016; Larkin et al., 2017; He and Huang, 2018), it is essential to build models that are able to distinguish the changes caused by these effects from the ones induced by the lockdown measures. Several studies have noted that incomplete correction for meteorological conditions could lead to biased results (Menut et al., 2020; Xiang et al., 2020). The CTMs can address this problem by performing specific sensitivity tests on the input parameters and by simulating pollutant concentrations using different emission scenarios, such as "business as usual" versus "COVID-19"-specific emissions reflecting lockdown restrictive measures (Barré et al., 2020; Huang et al., 2020; Menut et al., 2020; Putaud et al., 2020). However, CTM simulations are computationally demanding and time consuming.

Several statistical models and machine learning algorithms were used to build a relationship between the pollutant concentrations at the monitoring stations and historical meteorological conditions, including multiple linear regression (Venter et al., 2020), gradient boosting (Barré et al., 2020) and random forest (Dobson and Semple, 2020; Shi et al., 2021). The resulting models were used to predict the weather-normalized pollutant concentrations during the lockdown and to compare these estimates to the observed data. Giani et al. (2020) used a geostatistical model, incorporating CTM simulations as covariate, to predict and compare gridded $PM_{2.5}$ concentration in 2016–2019 and during the COVID-19 outbreak in 2020. A different way to model the effect of lockdown within a statistical formulation, which can fully quantify the uncertainty in the estimated effect, is by introducing the lockdown period as a covariate in the model. In Liu et al. (2020), two different government's responses to COVID-19 pandemic were assessed by using a fixed-effects model that predicts NO_2 tropospheric vertical column density (TVCD) before and after the 2020 Lunar New Year (LNY) in China, while controlling for the previous years' (2015–2019) NO_2 TVCD. This allowed distinguishing between the reductions typically observed during LNY and the ones caused by the lockdown measures. However, the model did not consider spatio-temporal correlations in the data and, therefore, the estimates of the statistical significance of the effects of covariates might be biased. In addition, the results represent changes in tropospheric NO_2 concentration, a proxy that may not fully reflect the variations in the air pollution levels close to the surface.

Here, we developed Bayesian spatio-temporal (BST) regression models that assess changes in the surface NO_2 and $PM_{2.5}$ concentration across Europe during the first 20 weeks in 2020, while taking into account the spatio-temporal correlation present in the monitoring data. In particular, we propose two different modelling formulations that assess the effect of the lockdown measures on the variation in the weekly-averaged NO_2 and $PM_{2.5}$ concentrations. The first approach compares changes in pollutant concentrations in 2020 with the ones that happened during the same period in the previous five years, by introducing an offset term, which controls for the long-term average concentrations of each pollutant during 2014–2019. The model assumes that the meteorological and other factors in 2020 were the same as in the previous years and therefore the changes observed in 2020, are strictly due to the lockdown. The second approach models only the 2020 data, but it takes into account confounding factors that may influence the spatio-temporal distribution of each pollutant and therefore separates the effect of lockdown from the effects of confounders. Our modelling endeavours improve the estimation of the actual effect of lockdown on the air pollution burden across the European continent.

2. Materials and methods

2.1. Study area and data

The raw NO_2 and $PM_{2.5}$ measurements were obtained from the Air Quality e-Reporting database (Air Quality e-Reporting, 2020) maintained through the European environment information and observation network (Eionet). For the years 2019 and 2020, the up-to-date (E2a) air pollution monitoring data was used, whereas for 2014–2018, the more detailed historic dataflow (E1a) was considered. The E2a data are updated daily and are available on hourly basis for most of European Union (EU) member states and European Environment Agency's (EEA's) cooperating countries. The E1a data are reported every September and cover the year before the delivery. The measurements as well as the meta-information on the monitoring stations involved were accessed from the EEA's air quality portal (<https://discomap.eea.europa.eu/map/fme/AirQualityExport.htm>). All the analyses were based on weekly averaged 24 h concentrations during the first 20 weeks of each year (e.g. for 2020 this period corresponds to 01/01/2020–15/05/2020). The stations with valid measurements for at least

19 out of 20 weeks were used in all further analyses. For storing raster data, statistical inference and mapping purposes all data was converted to the Lambert Azimuthal Equal Area (ETRS89-LAEA5210) projection. Fig. 1 illustrates the locations of the (a) NO_2 and (b) $\text{PM}_{2.5}$ monitoring sites used in this work.

Most of the data-driven air-quality modelling efforts incorporate air pollution proxies from satellite-based observations and/or chemical transport model simulations in the analyses (Benas et al., 2013; Beloconi et al., 2016; Brauer et al., 2016; Liu et al., 2020). These proxies reflect contributions from all sources, including e.g. emissions from industry, roads, airports or harbours, as well as atmospheric and weather conditions (Novotny et al., 2011). Since we were interested in evaluating the impact of climatic and environmental factors on air pollutants separately and in quantifying how they influence the effect of lockdown, the satellite-based observations and CTM simulation data were not included in the current analyses. Instead, the parameters that directly contribute to NO_2 and $\text{PM}_{2.5}$ formation and dispersion (and therefore drive their spatio-temporal variation), were used as separate covariates in the models following our previous works (Beloconi et al., 2018; Beloconi and Vounatsou, 2020) and based on the literature review and data availability at continental scale.

The land-use/cover data were extracted from the pan-European component of the Copernicus land monitoring service (CLMS, 2020). In particular, the CORINE land cover (CLC) dataset for the year 2012 was used (Corine Land Cover, 2012). To better understand the urban surface characteristics surrounding each monitoring station, a squared buffer zone of 1 km^2 spatial resolution was created and the dominant CLC category within each buffer zone was computed and assigned to the respective site. The 45 land classes available in CLC were aggregated to form the following 4 main categories: (i) continuous urban fabric - road and rail networks and associated land - port areas (LC1); (ii) discontinuous urban fabric - industrial or commercial units - mine, dump and construction sites - artificial, non-agricultural vegetated areas (LC2); (iii) agricultural areas - wetlands - water bodies (LC3); and (iv) forest and semi natural areas (LC4). Additionally, the high resolution layers of tree cover density (TCD, 2015), imperviousness density (IMP, 2015) and European settlement map (ESM, 2016) were accessed from the same source (CLMS, 2020). The digital elevation model (*Digital*

Elevation Model Over Europe (EU-DEM), 2017) product was downloaded from the EEA website.

The normalized difference vegetation index (NDVI, 2020) generated from the MODIS Aqua and Terra platforms, the night time lights (NTL, 2013) product from the National Oceanic and Atmospheric Administration (NOAA), as well as the climatic data from the National Centers for Environmental Prediction (NCEP) Climate Forecast System (CFSv2) (Saha et al., 2011) were pre-processed in Google Earth Engine (GEE) API (Google Earth Engine Team, 2015). The road density (RD) raster was computed using the OpenStreetMap project's collection (extracted in February 2016) of road shapefiles covering the continent. Particularly, the major roads comprising the motorway, trunk, primary and secondary road categories, as well as the links between them were taken into consideration. The same dataset was used to compute the distance to roads (DISR) covariate applying simple GIS (Geographic Information System) techniques. Since only the major roads were used in the computations, we do not expect significant changes in these estimates compared to 2020. Distance to sea (DISS) was calculated using the Europe coastline shapefile (*Europe Coastline Shapefile, 2015*) downloaded from the EEA website. The dust covariate (DUST) was derived from the ensemble of pan-European chemical transport models (Inness et al., 2019) of the Copernicus atmosphere monitoring service (CAMS, 2020a). Table 1 summarizes the covariates used in the models. A B-spline curve with 7 degrees of freedom was fitted to the pollutant data and the above time-varying parameters to graphically compare the temporal trends.

The week that the governments of each European country introduced the first major policy to tackle the spread of the virus was obtained from the ACAPS COVID-19 government measures dataset (<https://www.acaps.org/covid19-government-measures-dataset>). For most of the countries, the "Border closure" measure belonging to the "Movement restrictions" category was used to define the lockdown. The earliest date of this measure was considered and a value of 1 was assigned to the country-specific weekly lockdown variable for that and subsequent weeks; the value of 0 was allocated otherwise. For UK, Malta and the Netherlands the date of this particular measure was not available, therefore we used the dates of the "Surveillance and monitoring", "International flight suspension" and "Social distancing"

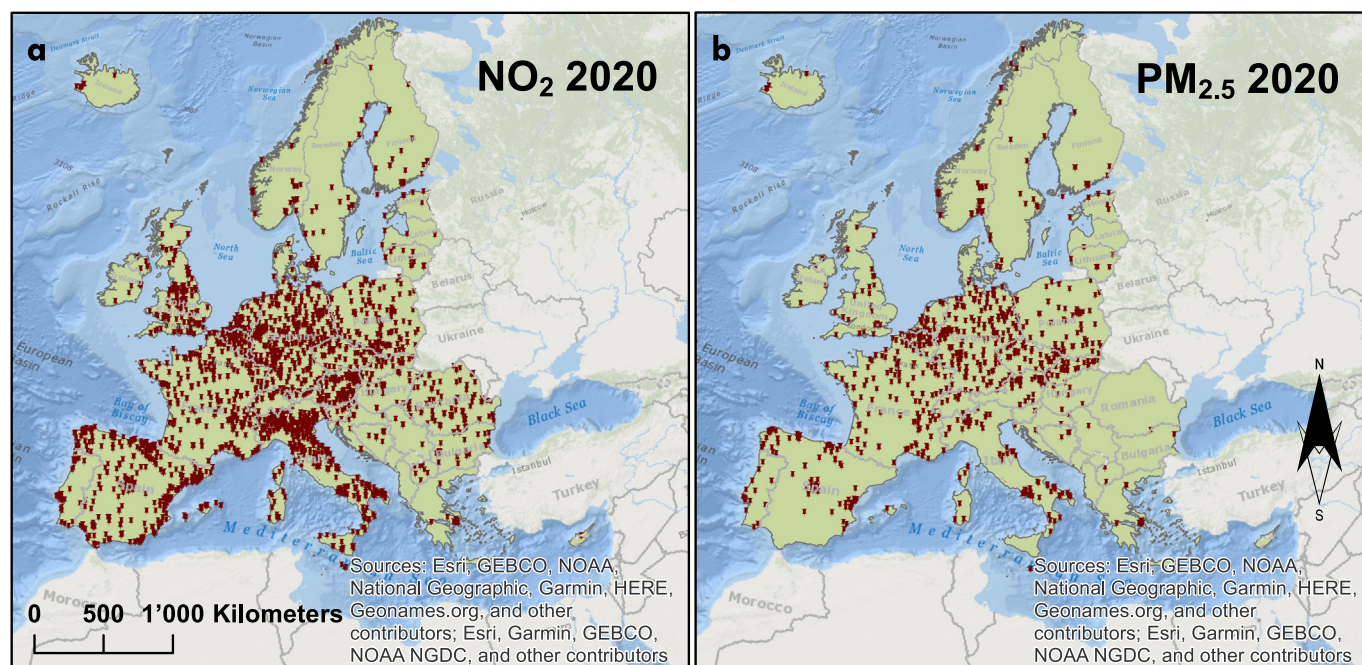


Fig. 1. Study area and monitoring network. The location of the 2672 NO_2 (a) and 947 $\text{PM}_{2.5}$ (b) monitoring stations in 2020 used in this work.

Table 1
Data sources and spatio-temporal resolution of the covariates used in our models.

Product	Temporal resolution	Spatial resolution	Source
Corine Land Cover (LC)	Year 2012	100 m × 100 m	CLMS
Tree Cover Density (TCD)	Year 2015	20 m × 20 m	CLMS
Imperviousness (IMP)	Year 2015	20 m × 20 m	CLMS
European Settlement Map (ESM)	Year 2016	100 m × 100 m	CLMS
Digital Elevation Model (DEM)	Year 2000	30 m × 30 m	EEA
Night Time Lights (NTL)	Year 2013	1 km × 1 km	NOAA
Road Density (RD)	February 2016	1 km × 1 km	OpenStreet Maps
Distance to Roads (DISR)	February 2016	Vector	OpenStreet Maps
Distance to Sea (DISS)	Year 2015	Vector	EEA
Normalized Difference Vegetation Index (NDVI)	2 acquisitions per day	1 km × 1 km	MODIS Aqua and Terra
Precipitation (PREC)	Every 6 h	0.2° × 0.2°	NCEP/CFSv2
Specific Humidity (SHUM)	Every 6 h	0.2° × 0.2°	NCEP/CFSv2
Wind Speed (WINDSP)	Every 6 h	0.2° × 0.2°	NCEP/CFSv2
Dust (DUST)	Hourly	0.1° × 0.1°	CAMS - Ensemble

measures, respectively to define the week of the lockdown. We note that no country has lifted the lockdown before the end date of the investigated period, i.e. the 15th of April.

2.2. Bayesian spatio-temporal modelling

To analyse the effects of the lockdown policies, we developed Bayesian spatio-temporal regression models that take into account the spatial and temporal correlation present in the data. The spatial correlation was modelled by location-specific random effects through a Gaussian process which captures the spatial correlation via the covariance matrix as a function of distance between locations. For the temporal component, an autoregressive (AR) structure was assumed.

Let $y(\mathbf{s}_j, t)$ denote the realization of a spatio-temporal process $Y(\cdot, \cdot)$ that represents the log-observed weekly averaged NO_2 or $PM_{2.5}$ concentration in 2020 during week $t = 1, \dots, 20$ at station $j = 1, \dots, N_t \in D \subseteq \mathbb{R}^2$ (location \mathbf{s}_j). We assume the following two model formulations (M1 and M2) for each pollutant:

$$y(\mathbf{s}_j, t) = \bar{y}_{2014-2019}(\mathbf{s}_j, t) + \beta_0^{(M1)} + X(\mathbf{s}_j, t)\beta_L^{(M1)} + \xi^{(M1)}(\mathbf{s}_j, t) + \varepsilon^{(M1)}(\mathbf{s}_j, t) \quad (1)$$

and

$$y(\mathbf{s}_j, t) = \beta_0^{(M2)} + X(\mathbf{s}_j, t)\beta_L^{(M2)} + \mathbf{z}(\mathbf{s}_j, t)\boldsymbol{\beta}^{(M2)} + \xi^{(M2)}(\mathbf{s}_j, t) + \varepsilon^{(M2)}(\mathbf{s}_j, t) \quad (2)$$

where the superscripts (M1) and (M2) distinguish between the two models, $\bar{y}_{2014-2019}(\mathbf{s}_j, t)$, i.e. $\bar{y}_{2014-2019}(\mathbf{s}_j, t) = \frac{1}{6} \sum_{year=2014}^{2019} y_{year}(\mathbf{s}_j, t)$ is an offset term representing the log-observed average pollutant concentration during 2014–2019 for site \mathbf{s}_j and week t , β_0 is the intercept, β_L is the coefficient associated with the lockdown $X(\mathbf{s}_j, t)$, $\mathbf{z}(\mathbf{s}_j, t) = (z_1(\mathbf{s}_j, t), \dots, z_p(\mathbf{s}_j, t))^T$ is the vector of additional p covariates for site \mathbf{s}_j and week t , $\boldsymbol{\beta} = (\beta_1, \dots, \beta_p)^T$ is the vector of the corresponding coefficients, $\xi(\mathbf{s}_j, t)$ represents the realization of the spatio-temporal process and $\varepsilon(\mathbf{s}_j, t)$ is the measurement error, that is considered both temporally and spatially uncorrelated.

The first formulation (Eq. (1)) compares the changes in pollutant concentrations in 2020 with the ones that happened during the same period in previous years: the offset term $\bar{y}_{2014-2019}$ introduced in the model controls for the long term average concentration during 2014–2019. In order to obtain more stable results, only the monitoring stations for which at least 3 years (out of these six preceding 2020) have non-missing weekly measurements were kept. The second formulation (Eq. (2)) models only the 2020 data but takes into account confounding factors influencing the spatio-temporal distribution of each pollutant: the vector $\mathbf{z}(\mathbf{s}_j, t)$ represents the covariates shown in Table 1, extracted at the locations of the monitoring stations. All the continuous covariates were standardized by subtracting the mean and dividing by the standard deviation (calculated using the 20-week measurements from all

the monitoring stations). In both modelling frameworks, the lockdown effect is introduced in the model as a location-specific binary variable $X(\mathbf{s}_j, t)$ indicating the pre- and post- “intervention” periods.

The spatio-temporal correlation structure is considered to be the same for both formulations. In particular, the realization $\xi(\mathbf{s}_j, t)$ is assumed to be a spatio-temporal Gaussian field that changes in time according to a first order autoregressive process $AR(1)$, with temporal correlation ρ , such as $|\rho| < 1$, that is

$$\xi(\mathbf{s}_i, t) = \rho \xi(\mathbf{s}_i, t-1) + \omega(\mathbf{s}_i, t) \text{ for } t = 1, \dots, 20 \text{ and } \xi(\mathbf{s}_i, 1) \sim \mathcal{N}\left(0, \frac{\sigma_\omega^2}{1-\rho^2}\right) \quad (3)$$

The $\omega(\mathbf{s}_i, t) = (\omega(s_{i1}, t), \dots, \omega(s_{iN_t}, t))^T$ is a spatial random effect that is assumed to arise from a multivariate normal distribution $\boldsymbol{\omega} \sim \mathcal{N}(\mathbf{0}_{N_t}, \sigma_\omega^2 \boldsymbol{\Sigma}_\omega)$ with $\mathbf{0}_{N_t}$ a $N_t \times 1$ zeros vector, σ_ω^2 the spatial process variance and $\boldsymbol{\Sigma}_\omega$ the $N_t \times N_t$ dense correlation matrix with elements $(\boldsymbol{\Sigma}_\omega)_{ij} = C(\|\mathbf{s}_i - \mathbf{s}_j\|)$. $C(\cdot)$ is the Matern function given by $C(d_{ij}) = \frac{1}{\Gamma(\nu)^2} (\kappa d_{ij})^\nu K_\nu(\kappa d_{ij})$ with d_{ij} the distance between stations i and j , κ is a scaling parameter, ν is a smoothing parameter (fixed to 1 in our application) and K_ν is the modified Bessel function of second kind and order ν . This specification implies that the range r (the distance at which the spatial variance becomes less than 10%) is given by $r = \sqrt{8\nu}/\kappa$.

To evaluate whether modelling the spatial and spatio-temporal correlation present in the data leads to a better model fit, and therefore more accurate estimates of the effect of the lockdown (and other covariates), the aforementioned formulations were compared to the ones in which these auto-correlations are not taken into consideration. Bayesian model selection measures (Gelman et al., 2014), including the deviance information criterion (DIC) (Spiegelhalter et al., 2002), the widely applicable Bayesian information criterion (WAIC) (Watanabe, 2013) and the logarithmic score (logscore) (Ntzoufras, 2008) were used to compare the models. Lower values of these measures indicate a better model fit.

The Bayesian model formulation is completed by specifying prior distributions for the parameters and the hyperparameters. Particularly, the log-gamma priors were chosen for the σ_ε^{-2} , σ_ω^{-2} and r was parameterized on the log-scale, i.e.: $\log(\sigma_\varepsilon^{-2}), \log(\sigma_\omega^{-2}) \sim \log Ga(1, 5 \cdot 10^{-5})$ and $\log(r) \sim \log Ga(1, 10^2)$. Normal priors $\mathcal{N}(0, 10^3)$ were assigned to the regression coefficients, a vague normal one for the intercept and a $\mathcal{N}(0, 0.15)$ prior for the log-transformed autoregressive coefficient ρ , $\log\left(\frac{1+\rho}{1-\rho}\right)$.

Model fit was carried out using the stochastic partial differential equations (SPDE) method and the integrated nested Laplace approximation (INLA) algorithm (Rue et al., 2009; Lindgren et al., 2011) for

fast approximation of the marginal posterior distributions. In the SPDE/INLA approach, the spatial process is approximated by a Gaussian Markov random field (GMRF) with zero mean and a symmetric positive definite precision matrix Q (defined as the inverse of $\Sigma_{\omega} = \sigma_{\omega}^2 \mathbf{R}_{\omega}$). First, a GMRF representation of the Matern field is constructed on a set of non-intersecting triangles partitioning the domain of the study area (Lindgren et al., 2011). Subsequently, the INLA algorithm estimates the posterior distribution of the latent Gaussian process and hyperparameters using the Laplace approximation (Rue et al., 2009). More details regarding this methodology are provided elsewhere (Blangiardo and Cameletti, 2015). All the models were fitted on an Intel Xeon E5-2697 CPU machine (2×2.60 GHz, 128 GB RAM) using the R-INLA package (Rue et al., 2013) available within the R software (R Core Team, 2015).

Parameter estimates were summarized by their posterior medians and the corresponding 95% Bayesian Credible Intervals (BCI). The effect of a covariate was considered to be statistically important if its 95% BCI did not include zero. We use the term statistically important rather than statistically significant as the latter is not applicable to Bayesian inference.

3. Results

3.1. Data observed at the monitoring stations

Fig. 2 depicts weekly averaged concentration of NO_2 and $\text{PM}_{2.5}$ observed at the location of the monitoring stations across Europe during

the first 20 weeks in 2020 (blue dots). To explore whether these differences in surface concentration are typically observed during the investigated period, we further depict the measurements of both pollutants obtained in 2014–2019 (red dots) together with B-spline curves fitted to each combination of pollutant/year(s). The shaded areas represent the approximate 95% confidence intervals of each fitted spline.

Consistent with the 2014–2019 data, NO_2 concentration increases during the first 4 weeks in 2020 and starts decreasing after week 5. The similarities in the $\text{PM}_{2.5}$ levels between the current and the previous years are less homogeneous. In general, the concentration of both pollutants is lower in 2020 compared to the average observed in previous years. The lockdown measures that are considered here, are mostly related to border closures (part of the “Movement restrictions” interventions) and have occurred in most European countries between week 10 and 13. One can see that the NO_2 concentrations declined more abruptly during 2020, compared to previous years, whereas the $\text{PM}_{2.5}$ concentrations remained rather stable (even slightly increased). Additionally, both pollutants have shown a small rebound in mean concentrations after week 18.

3.2. Bayesian spatio-temporal models

Bayesian models were fitted to better understand the factors that are related to changes in the concentrations of NO_2 and $\text{PM}_{2.5}$ in 2020 compared to previous years and to assess whether they are directly influenced by the lockdown policies or other factors that affect the

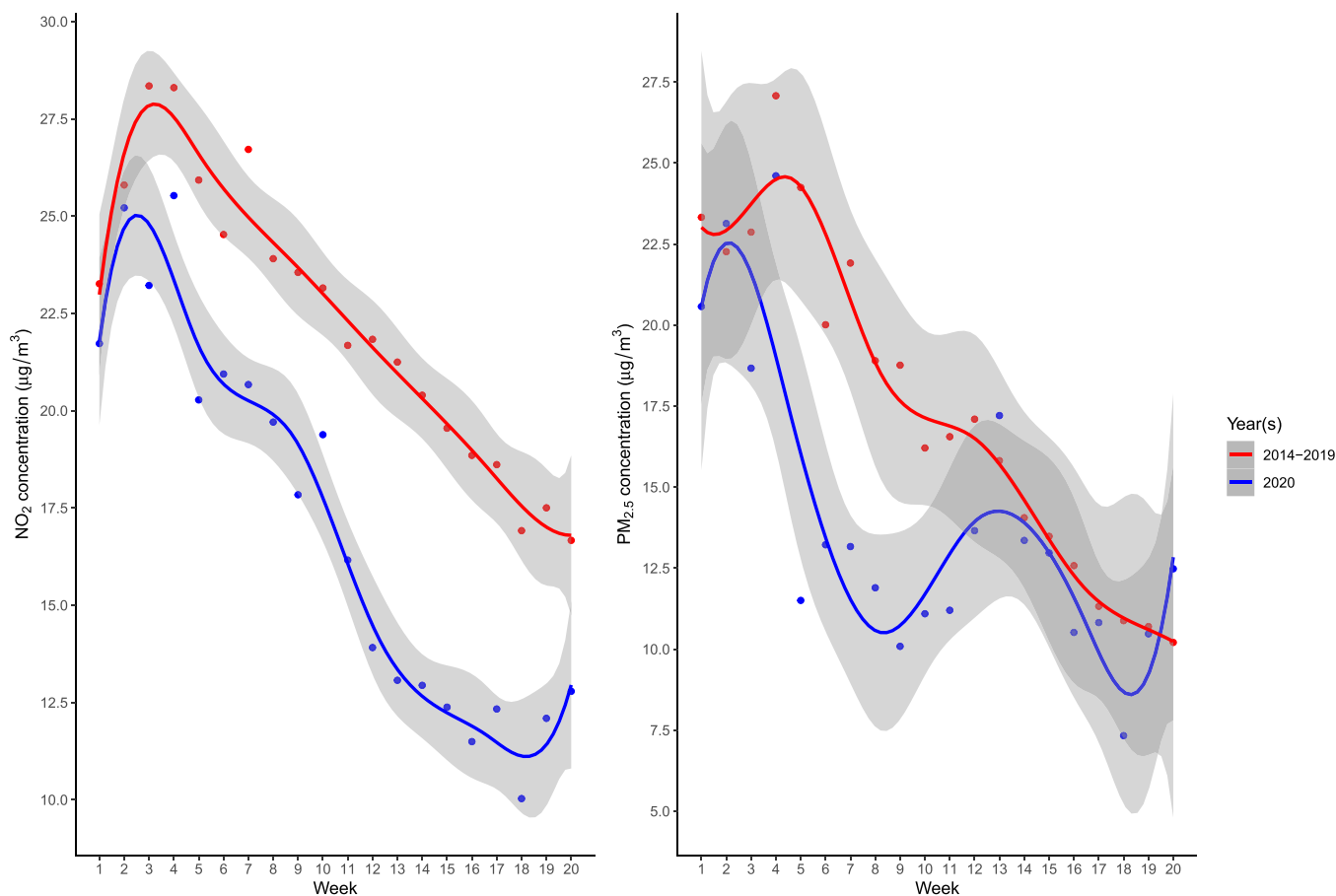


Fig. 2. Weekly variations in the NO_2 (left) and $\text{PM}_{2.5}$ (right) concentration. Dots denote the weekly averaged concentration of NO_2 and $\text{PM}_{2.5}$ observed at the monitoring stations across Europe during the first 20 weeks of 2020 (blue dots) and 2014–2019 (red dots). A B-spline curve with 7 degrees of freedom was fitted to each combination of pollutant/year(s). Shaded areas represent the approximate 95% confidence intervals of each fitted spline.

formation, dispersion and transportation of each pollutant (such as meteorological conditions).

Model M1 compares the changes in pollutant concentrations in 2020 with the ones that happened during the same period in previous years, by introducing an offset term that controls for the long term average concentration over the last 6 years before 2020 (Eq. (1)). Parameter estimates of the three formulations, i.e. (i) spatio-temporal ($M1^{ST}$); (ii) spatial ($M1^S$); and (iii) independent correlation structure ($M1^0$) are shown in Tables 2 and 3 for NO_2 and $PM_{2.5}$, respectively. For both pollutants the spatio-temporal model fitted the data the best as indicated by the lower logscore, DIC and WAIC values.

The negative intercept ($\beta_0^{(M1)}$) estimated for each of the two pollutants proposes that their concentration dropped in 2020 when compared to the previous years, a result that is consistent with the pattern of the raw data shown in Fig. 2. Results regarding the estimated coefficient of the lockdown covariate ($\beta_L^{(M1)}$) differ between the two pollutants. The coefficient of NO_2 is negative, indicating that on average, during the lockdown period, the concentration dropped by 6% more than in the previous years.

Similarly, the positive coefficient estimated for $PM_{2.5}$ indicates that in comparison to previous years, we see a 15% increase in the concentrations during the lockdown period. This result is consistent with the increase in $PM_{2.5}$ in 2020 noticed during the weeks 10–15 in Fig. 2, reaching similar concentrations as in the 2014–2019 period, and not observed during the same time-frame in previous years.

To evaluate whether the changes observed during lockdown are driven by other factors, such as weather conditions, local emission/combustion sources and land surface characteristics, we use the M2 model (Eq. (2)), which analyses only the 2020 data and takes into account proxies of the above-mentioned confounding factors.

Fig. 3 shows the variation in the climatic and environmental factors that occurred at the location of the monitoring stations across Europe during the first 20 weeks in 2020. The results of model fit for the M2 formulations are shown in Tables 4 and 5 for NO_2 and $PM_{2.5}$, respectively. Similarly to the M1 framework, the Bayesian model selection criteria indicate that the spatio-temporal models ($M2^{ST}$) perform best for both pollutants. The DIC, WAIC and logscore metrics for M2 are not directly comparable to those from M1, because the models were fitted on a different number of observations. M1 included data from monitoring stations with at least 3 years (out of the 6 preceding 2020) non-missing

Table 2

Posterior medians, 95% Bayesian credible intervals (BCI) and model fit metrics of the M1 formulation fitted to surface NO_2 concentrations. $M1^{ST}$, $M1^S$ and $M1^0$ denote the spatio-temporal, spatial and independent model, respectively.

Covariates	M1⁰	M1^S (Space)	M1ST (Space-Time)
	Median (95% BCI)	Median (95% BCI)	Median (95% BCI)
Intercept ($\beta_0^{(M1)}$)	-0.285 (-0.290, -0.280)	-0.239 (-0.250, -0.229)	-0.233 (-0.244, -0.223)
Lockdown ($\beta_L^{(M1)}$)	-0.207 (-0.214, -0.200)	-0.091 (-0.106, -0.075)	-0.082 (-0.097, -0.067)
(1) σ_ϵ^2	0.16 (0.16, 0.17)	0.13 (0.12, 0.13)	0.12 (0.12, 0.12)
(2) σ_w^2	-	0.05 (0.05, 0.06)	0.39 (0.31, 0.49)
(3) r (km)	-	809.5 (746.7, 881.9)	703.7 (640.8, 784.9)
(4) ρ	-	-	0.974 (0.967, 0.979)
(5) DIC	48,697.4	37,924.1	34,411.0
(6) WAIC	48,699.8	37,947.0	34,330.5
(7) logscore	0.515	0.402	0.363

(1) σ_ϵ^2 – variance of the random error; (2) σ_w^2 – variance of the spatial process; (3) r – range; (4) ρ – coefficient of AR(1).

(5) DIC – deviance information criterion; (6) WAIC – Widely applicable Bayesian information criterion; (7) logscore – logarithmic score.

$\log NO_2 = \log(\overline{NO_2})_{2014-2019} - 0.233 - 0.082 \cdot X(\mathbf{s}_j, t)$ results in $NO_2 = 0.73 \cdot (\overline{NO_2})_{2014-2019}$ after the lockdown (i.e. when $X(\mathbf{s}_j, t) = 1$) and $NO_2 = 0.79 \cdot (\overline{NO_2})_{2014-2019}$ otherwise (i.e. when $X(\mathbf{s}_j, t) = 0$); $M1^0$ – independent model; $M1^S$ – spatial model; $M1^{ST}$ – spatio-temporal model.

Table 3

Posterior medians, 95% Bayesian credible intervals (BCI) and model fit metrics of the M1 formulation fitted to surface $PM_{2.5}$ concentrations. $M1^{ST}$, $M1^S$ and $M1^0$ denote the spatio-temporal, spatial and independent model, respectively.

Covariates	M1⁰	M1^S (Space)	M1ST (Space-Time)
	Median (95% BCI)	Median (95% BCI)	Median (95% BCI)
Intercept ($\beta_0^{(M1)}$)	-0.471 (-0.482, -0.461)	-0.377 (-0.392, -0.362)	-0.371 (-0.386, -0.356)
Lockdown ($\beta_L^{(M1)}$)	0.331 (0.315, 0.348)	0.209 (0.187, 0.230)	0.201 (0.179, 0.222)
(1) σ_ϵ^2	0.26 (0.26, 0.27)	0.14 (0.14, 0.15)	0.14 (0.13, 0.14)
(2) σ_w^2	-	0.13 (0.12, 0.15)	0.39 (0.33, 0.48)
(3) r (km)	-	819.0 (739.6, 936.8)	1039.5 (807.8, 1204.0)
(4) ρ	-	-	0.879 (0.860, 0.903)
(5) DIC	22,699.3	14,623.5	13,783.6
(6) WAIC	22,700.0	14,486.1	13,628.9
(7) logscore	0.749	0.480	0.451

(1) σ_ϵ^2 – variance of the random error; (2) σ_w^2 – variance of the spatial process; (3) r – range; (4) ρ – coefficient of AR(1).

(5) DIC – deviance information criterion; (6) WAIC – Widely applicable Bayesian information criterion; (7) logscore – logarithmic score.

$M1^0$ – independent model; $M1^S$ – spatial model; $M1^{ST}$ – spatio-temporal model.

weekly measurements, while M2 formulations included data from more monitoring sites available in 2020.

Most of the covariates included in the models have a statistically important regression coefficient (Tables 4–5). The directions of the effects (i.e. the positive/negative associations) are mostly consistent with our previous works (Beloconi et al., 2018; Beloconi and Vounatsou, 2020). Thus e.g. elevation (DEM), wind speed (WINDSP) and surface humidity (SHUM) have an important negative effect on NO_2 and $PM_{2.5}$, while the distance to the sea (DISS) and the night time lights (NTL) are positively associated with both pollutants. In addition to our previous works, here we found an important positive association of the dust covariate (DUST) with each outcome.

The M2 framework resulted in a negative important coefficient of the lockdown variable for both pollutants. In particular, the negative coefficient $\beta_L^{(M2)} = -0.35$ estimated for NO_2 , implies that the concentration of NO_2 has dropped on average by 29.5% due to the lockdown (i.e. $\log NO_2^{(L1)} - \log NO_2^{(L0)} = -0.35$ during lockdown and therefore $NO_2^{(L1)} = 0.705 \cdot NO_2^{(L0)}$). The corresponding 95% BCI is (28.1%, 30.9%). Similarly, the negative coefficient estimated for $PM_{2.5}$ (i.e. $\beta_L^{(M2)} = -0.30$) indicates that the governments' interventions resulted in a 25.9% (23.6%, 28.1%) drop in the pollutant concentration on average across the continent (here $PM_{2.5}^{(L1)} = 0.741 \cdot PM_{2.5}^{(L0)}$).

4. Discussion

The demand for rigorous spatio-temporal models that are able to accurately assess the impact of policy interventions has rapidly grown over the past decade. This need became more pronounced during the last year, following the start of the COVID-19 pandemic where a large number of interventions have been implemented by different countries. Here we developed and evaluated different model formulations to quantify the effect of the lockdown policy on the air quality in Europe. To our knowledge, this research is the first to account for the spatio-temporal correlation present in the monitoring data during the pandemic and to assess how it affects estimation of the lockdown effect while accounting for confounding factors.

A critical review on the early studies assessing the nexus between COVID-19 and the environment (Shakil et al., 2020) has shown that, in terms of methodology, the majority of the first articles examining the impacts of COVID-19 on air pollution have used explorative analyses, such as graphical comparisons. As noted by the authors, these analyses had limitations to postulate robust findings. They were rather descriptive and therefore the inferences were limited to theoretical or empirical explanations of the research problem. In particular, these

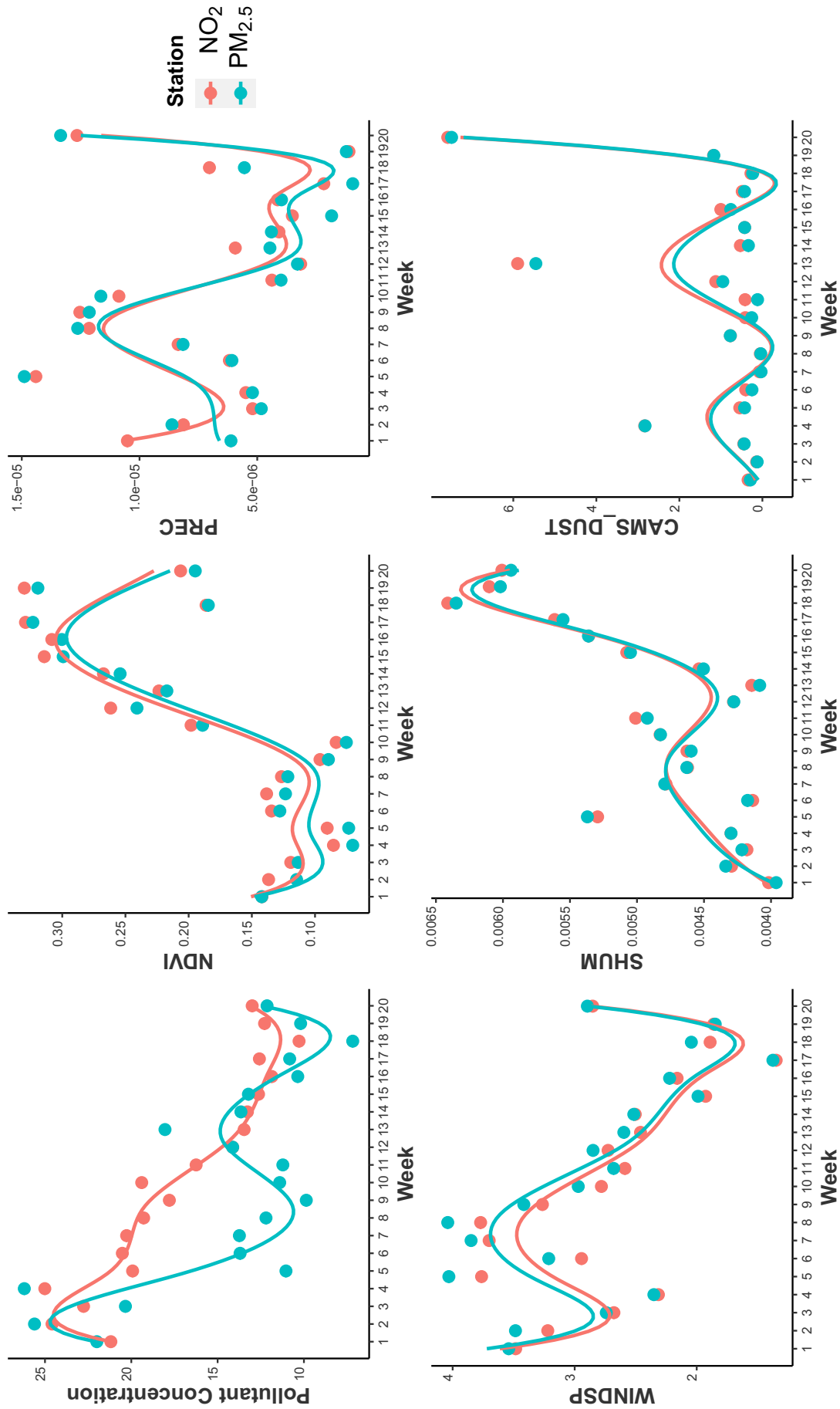


Fig. 3. Weekly variations in the pollutants' concentrations and the time-dependent covariates observed at the locations of the NO₂ and PM_{2.5} monitoring stations across Europe. Dots denote the weekly averaged values during the first 20 weeks of 2020. A B-spline curve with 7 degrees of freedom was fitted to each data time series.

Table 4

Posterior medians, 95% Bayesian credible intervals (BCI) and model fit metrics of the $M2$ formulation fitted to surface NO_2 concentrations. $M2^{ST}$, $M2^S$ and $M2^0$ denote the spatio-temporal, spatial and independent model, respectively.

Covariates	$M2^0$	$M2^S$ (Space)	$M2^{ST}$ (Space-Time)
	Median (95% BCI)	Median (95% BCI)	Median (95% BCI)
Intercept ($\beta_0^{(M2)}$)	2.93 (2.91, 2.94)	2.93 (2.91, 2.90)	2.92 (2.90, 2.94)
Lockdown ($\beta_1^{(M2)}$)	-0.51 (-0.52, -0.50)	-0.41 (-0.43, -0.38)	-0.35 (-0.37, -0.33)
TCD	0.01 (0.01, 0.02)	0.01 (-0.00, 0.01)	0.01 (-0.00, 0.01)
IMP	0.11 (0.10, 0.11)	0.10 (0.09, 0.11)	0.10 (0.09, 0.11)
ESM	0.00 (0.00, 0.01)	0.01 (0.00, 0.01)	0.01 (0.01, 0.02)
DEM	-0.13 (-0.14, -0.13)	-0.11 (-0.12, -0.11)	-0.11 (-0.11, -0.10)
NTL	0.28 (0.28, 0.29)	0.29 (0.28, 0.30)	0.30 (0.29, 0.30)
RD	0.06 (0.05, 0.06)	0.07 (0.06, 0.07)	0.07 (0.07, 0.08)
DISS	0.13 (0.12, 0.13)	0.11 (0.11, 0.12)	0.11 (0.10, 0.11)
DISR	-0.04 (-0.05, -0.04)	-0.04 (-0.05, -0.04)	-0.04 (-0.05, -0.04)
NDVI	0.01 (0.00, 0.01)	-0.01 (-0.01, 0.00)	0.00 (-0.01, 0.01)
PREC	-0.01 (-0.02, -0.01)	-0.02 (-0.02, -0.01)	-0.02 (-0.02, -0.01)
SHUM	-0.19 (-0.19, -0.18)	-0.13 (-0.14, -0.12)	-0.11 (-0.12, -0.10)
WINDSP	-0.17 (-0.18, -0.17)	-0.17 (-0.18, -0.17)	-0.17 (-0.18, -0.17)
DUST	0.03 (0.03, 0.04)	0.02 (0.01, 0.02)	0.02 (0.01, 0.02)
LC			
LC2	-0.11 (-0.13, -0.10)	-0.12 (-0.14, -0.11)	-0.11 (-0.13, -0.10)
LC3	-0.15 (-0.17, -0.13)	-0.16 (-0.18, -0.14)	-0.15 (-0.17, -0.13)
LC4	-0.43 (-0.45, -0.40)	-0.40 (-0.42, -0.37)	-0.36 (-0.38, -0.33)
⁽¹⁾ σ_e^2	0.29 (0.29, 0.29)	0.25 (0.25, 0.25)	0.22 (0.21, 0.22)
⁽²⁾ σ_w^2	-	0.06 (0.05, 0.06)	6.54 (5.44, 8.32)
⁽³⁾ r (km)	-	667.6 (600.1, 753.9)	1101.6 (965.7, 1237.2)
⁽⁴⁾ ρ	-	-	0.999 (0.999, 0.999)
⁽⁵⁾ DIC	84,430.7	78,136.9	70,390.2
⁽⁶⁾ WAIC	84,435.1	78,203.1	70,315.4
⁽⁷⁾ logscore	0.798	0.739	0.664

⁽¹⁾ σ_e^2 – variance of the random error; ⁽²⁾ σ_w^2 – variance of the spatial process; ⁽³⁾ r – range; ⁽⁴⁾ ρ – coefficient of AR(1).

⁽⁵⁾ DIC – deviance information criterion; ⁽⁶⁾ WAIC – Widely applicable Bayesian information criterion; ⁽⁷⁾ logscore – logarithmic score;

$M2^0$ – independent model; $M2^S$ – spatial model; $M2^{ST}$ – spatio-temporal model.

TCD – Tree Cover Density; IMP – Imperviousness; ESM – European Settlement Map; DEM – Digital Elevation Model; NTL – Night Time Lights; RD – Road Density; DISS – Distance to Sea, DISR – Distance to Roads; NDVI – Normalized Difference Vegetation Index; PREC – Precipitation; SHUM – Specific Humidity; WINDSP – Wind Speed; LC – Land Cover classes.

analyses could not differentiate between the changes in pollutant concentration that occurred due to the governmental actions from the ones due to natural weather conditions or other spatio-temporal characteristics, such as seasonality. More recent studies have noted that the results could be biased if meteorological conditions are not taken into account (Menut et al., 2020; Xiang et al., 2020). Modelling efforts that separate the lockdown effect from the effects of other factors influencing the variations in air pollution levels, can be grouped in three main categories: (i) CTM simulations of the pollutant concentrations comparing different emissions that reflect “business as usual” with “COVID-19” scenarios (e.g. Barré et al., 2020; Huang et al., 2020; Menut et al., 2020; Putaud et al., 2020); (ii) statistical or machine learning methods that “weather-normalize” or compare the predicted “de-weathered” trends in air pollutants with observations during the lockdown period (e.g. Barré et al., 2020; Dobson and Semple, 2020; Shi et al., 2021; Venter et al., 2020); and (iii) statistical formulations that introduce the lockdown period as a time-dependent covariate in the model (e.g. Liu et al., 2020). Whereas the use of CTMs can fully quantify

Table 5

Posterior medians, 95% Bayesian credible intervals (BCI) and model fit metrics of the $M2$ formulation fitted to surface $PM_{2.5}$ concentrations. $M2^{ST}$, $M2^S$ and $M2^0$ denote the spatio-temporal, spatial and independent model, respectively.

Covariates	$M2^0$	$M2^S$ (Space)	$M2^{ST}$ (Space-Time)
	Median (95% BCI)	Median (95% BCI)	Median (95% BCI)
Intercept ($\beta_0^{(M2)}$)	2.40 (2.38, 2.42)	2.46 (2.43, 2.48)	2.41 (2.38, 2.43)
Lockdown ($\beta_1^{(M2)}$)	-0.21 (-0.23, -0.19)	-0.32 (-0.35, -0.29)	-0.30 (-0.33, -0.27)
TCD	-0.03 (-0.04, -0.02)	-0.03 (-0.03, -0.02)	-0.02 (-0.03, -0.02)
IMP	-0.03 (-0.04, -0.02)	-0.03 (-0.04, -0.02)	-0.03 (-0.04, -0.02)
ESM	0.01 (-0.01, 0.02)	0.01 (0.00, 0.02)	0.03 (0.02, 0.04)
DEM	-0.09 (-0.10, -0.08)	-0.09 (-0.10, -0.08)	-0.10 (-0.11, -0.09)
NTL	0.10 (0.09, 0.12)	0.09 (0.08, 0.10)	0.10 (0.08, 0.11)
RD	-0.03 (-0.04, -0.02)	-0.03 (-0.03, -0.02)	-0.04 (-0.05, -0.03)
DISS	0.12 (0.11, 0.13)	0.17 (0.16, 0.18)	0.21 (0.20, 0.22)
DISR	0.05 (0.04, 0.06)	0.05 (0.04, 0.06)	0.05 (0.04, 0.06)
NDVI	0.09 (0.08, 0.10)	0.07 (0.06, 0.08)	0.06 (0.05, 0.06)
PREC	-0.09 (-0.10, -0.08)	-0.06 (-0.07, -0.06)	-0.05 (-0.06, -0.05)
SHUM	-0.12 (-0.13, -0.11)	-0.03 (-0.04, -0.02)	-0.04 (-0.05, -0.03)
WINDSP	-0.18 (-0.19, -0.17)	-0.15 (-0.16, -0.14)	-0.14 (-0.15, -0.13)
DUST	0.11 (0.10, 0.12)	0.08 (0.07, 0.09)	0.07 (0.06, 0.08)
LC			
LC2	-0.01 (-0.03, 0.01)	0.01 (-0.01, 0.03)	0.03 (0.01, 0.05)
LC3	-0.07 (-0.10, -0.03)	-0.07 (-0.10, -0.03)	-0.05 (-0.09, -0.01)
LC4	-0.20 (-0.25, -0.16)	-0.15 (-0.20, -0.11)	-0.08 (-0.13, -0.04)
⁽¹⁾ σ_e^2	0.28 (0.27, 0.29)	0.20 (0.20, 0.21)	0.18 (0.18, 0.18)
⁽²⁾ σ_w^2	-	0.11 (0.10, 0.13)	5.09 (3.56, 6.88)
⁽³⁾ r (km)	-	823.1 (749.1, 928.8)	1714.5 (1493.0, 2148.8)
⁽⁴⁾ ρ	-	-	0.994 (0.991, 0.996)
⁽⁵⁾ DIC	29,466.9	24,708.5	22,003.9
⁽⁶⁾ WAIC	29,472.0	24,629.7	21,848.3
⁽⁷⁾ logscore	0.783	0.655	0.580

⁽¹⁾ σ_e^2 – variance of the random error; ⁽²⁾ σ_w^2 – variance of the spatial process; ⁽³⁾ r – range; ⁽⁴⁾ ρ – coefficient of AR(1).

⁽⁵⁾ DIC – deviance information criterion; ⁽⁶⁾ WAIC – Widely applicable Bayesian information criterion; ⁽⁷⁾ logscore – logarithmic score.

$M2^0$ – independent model; $M2^S$ – spatial model; $M2^{ST}$ – spatio-temporal model.

TCD – Tree Cover Density; IMP – Imperviousness; ESM – European Settlement Map; DEM – Digital Elevation Model; NTL – Night Time Lights; RD – Road Density; DISS – Distance to Sea, DISR – Distance to Roads; NDVI – Normalized Difference Vegetation Index; PREC – Precipitation; SHUM – Specific Humidity; WINDSP – Wind Speed; LC – Land Cover classes.

the changes in the emissions and potential chemical processes, they are computationally very demanding and time-consuming. The advantage of the statistical models that include the lockdown as a covariate, when compared to formulations that predict the “de-weathered” pollutant concentrations, is that the uncertainty of the estimated effect can be fully quantified (through confidence intervals). In fact, when the effect is embedded in the model, there is no need to compare predictions before and after “intervention”, using t-test or similar methods. Furthermore, the models can separate the effect of the lockdown from the effects of confounding factors. However, the literature applying such formulations is rather sparse. Liu et al. (2020) recently explored how the COVID-19 policies in China were associated with reductions in daily tropospheric NO_2 measurements by using a fixed-effects model that incorporates a binary variable indicating the pre- and post-intervention periods and adjusting for the average pollution levels prior to lockdown. However, the proposed model did not account for the spatio-temporal correlation present in the data and evaluated the

changes in the tropospheric measurements rather than in the surface level NO_2 concentrations, which are more relevant for human health.

Here, we proposed two statistical modelling formulations that assess the effect of the lockdown measures and differentiate between the changes in pollutant concentration that occurred due to the governmental actions and those due to seasonality. The first approach (*M1*) compares the variation in air pollution during the lockdown period in 2020, with the one during the same period in previous years. The second approach (*M2*) models only the 2020 data, but it includes confounding factors influencing the spatio-temporal distribution of each pollutant, such as weather conditions and land surface characteristics. In both cases, the lockdown effect is introduced as a binary variable indicating the pre- and post- “intervention” periods. The models were fitted within the Bayesian framework and evaluated three assumptions regarding the correlation structure of the air pollution data, i.e. independence between observations (no correlation), spatial and spatio-temporal correlation. Bayesian model selection criteria have shown that, for both pollutants, the spatio-temporal formulation had the best fit to the data. Therefore, using this model to draw inferences regarding the effects of the lockdown on the NO_2 and $PM_{2.5}$ concentration is preferable, since it minimizes the bias in the statistical importance of the estimates.

Consistent to the other studies (Table A1 in the appendix), both formulations we have proposed suggest a significant drop in NO_2 concentration following the COVID-19 lockdown, while the spike observed in $PM_{2.5}$ during the period coinciding with governments’ “interventions” may be caused by other factors, unrelated to lockdown policies. The observed high variability in the climatic conditions and the environmental factors occurring at the locations of the monitoring stations across Europe during the first 20 weeks in 2020 (Fig. 3), suggests that the changes observed in both pollutants during the lockdown period are not only due to the lockdown effect. For most of the European countries, the lockdown occurred between weeks 10 and 13. Thus, the drop in wind speed and the increase in dust and NDVI observed during the same time frame could have contributed to the increase in $PM_{2.5}$ concentration, as indicated by the corresponding regression coefficients of *M2* (i.e. important negative coefficient of wind speed and important positive coefficients of dust and NDVI). Therefore, after adjusting for these factors, *M2* could capture a 25.9% (23.6%, 28.1%) lockdown-related reduction in $PM_{2.5}$ concentration, which could not be estimated by *M1*. Similarly, the smaller drop in NO_2 due to the lockdown-related measures estimated by *M1* is less reliable compared to a 29.5% (28.1%, 30.9%) decrease obtained by *M2*, since part of the increase in NO_2 during the lockdown is attributed to the natural weather variations.

Similar ranges in the average relative NO_2 reduction were recently estimated across the European continent using the Copernicus atmosphere monitoring service (CAMS, 2020a) chemical transport model with reference and lockdown simulation scenarios based on a newly developed emission inventory (CAMS, 2020b). This inventory is representative of the reductions in industry, road transport and aviation activities for most of the European countries during the lockdown period (Guevara et al., 2020). Estimates based on gradient boosting machine learning method using satellite retrievals from the tropospheric monitoring instrument (TROPOMI, Veeffkind et al., 2012) revealed a milder reduction (of ~ 23%) in tropospheric NO_2 levels (Barré et al., 2020). Giani et al. (2020) estimated a 20.4% reduction in $PM_{2.5}$ concentration between 2016–2019 and 2020 by comparing gridded $PM_{2.5}$ surfaces in Europe obtained by ordinary kriging, incorporating the weather research and forecasting (WRF-Chem) simulations (Powers et al., 2016) as covariate.

Despite the fact that we find a similar range of reductions in two pollutants (slightly higher decrease for NO_2 and lower for $PM_{2.5}$), the estimated regression coefficients in the *M2* formulation can partially reflect the differences in their sources of emissions. In Europe, the transport sector is the largest contributor to NO_x emissions, especially in urban areas, whereas *PM* is affected by more sources (such as desert

dust transport, wildfires, power plants, home heating, coal burning in electricity production) and is subject to secondary formation in the ambient air (EEA, 2016). The regression coefficients (Tables 4 and 5) indicate that there are both similarities and differences between NO_2 and $PM_{2.5}$ associations with the meteorological, land-use/cover and other environmental factors. Since all the covariates were standardized, the estimates can be directly compared. Thus, elevation (DEM) or wind speed (WINDSP) have a similar important negative association with both pollutants (posterior median of the regression coefficients of -0.11 vs -0.10 and of -0.17 vs -0.14 , respectively). On the other hand, the road density has a positive important association with NO_2 but not with $PM_{2.5}$ (posterior median of $+0.07$ vs -0.04), whereas the dust covariate (DUST), which serves as a direct source of $PM_{2.5}$ has much stronger positive association with $PM_{2.5}$ compared to NO_2 (posterior median of $+0.07$ vs. $+0.02$).

While our research improves the assessment of the effect of the COVID-19 lockdown on the air pollution burden across the European continent, the findings are not without limitations. In particular, we did not consider differences in the containment measures with regard to the expected impact on air quality, but rather a binary lockdown indicator (common across all the countries). Spatially varying coefficient (SVC) models (Gelfand et al., 2003) may capture the spatial variability of the lockdown effect by allowing its regression coefficient to vary smoothly over space and time. However, these models are computationally very demanding for continental scale analyses. The feasibility of their application and their ability to improve the fit to the data should be further evaluated. Last but not least, statistical models cannot fully allocate the estimated reduction to different emission sources and potential chemical processes. Chemical transport models with up-to-date emission inventories are most appropriate to address the above question.

5. Conclusions

Our research provides an insight into the NO_2 and $PM_{2.5}$ changes in Europe in early 2020. We found that, in general, the concentrations of both pollutants are lower in 2020 compared to the average observed in previous years. This may reflect in part the effects of Europe’s clean air policy package, which sets out objectives for reducing the health and environmental impacts of air pollution by 2030. Rigorous modelling suggests that the lockdown measures, implemented by many European countries to stop the spread of coronavirus, have highly contributed to a decrease in both pollutants in 2020 with slightly higher reductions in NO_2 concentrations compared to $PM_{2.5}$. This result demonstrates how fast considerable reduction in air pollution can be achieved through strict policies.

CRedit authorship contribution statement

Anton Beloconi: Conceptualization, Methodology, Software, Validation, Formal analysis, Investigation, Data curation, Writing – original draft, Writing – review & editing, Visualization. **Nicole M. Probst-Hensch:** Conceptualization, Methodology, Writing – review & editing. **Penelope Vounatsou:** Conceptualization, Methodology, Resources, Data curation, Writing – review & editing, Supervision, Project administration, Funding acquisition.

Declaration of competing interest

The authors declare that they have no known competing financial interests or personal relationships that could have appeared to influence the work reported in this paper.

Acknowledgements

Funding: This work was supported by the European Research Council (ERC) Advanced Grant [Project no. 323180]; and the Swiss

Federal Office for the Environment (FOEN) [Contract no. 17.0094.PJ/5666BF610]. The results of this study have been achieved incorporating data of the Copernicus Land Monitoring Service (CLMS) and of the Copernicus Atmosphere Monitoring Service (CAMS).

Appendix A. Supplementary data

Supplementary data to this article can be found online at <https://doi.org/10.1016/j.scitotenv.2021.147607>.

References

- Abdullah, S., Mansor, A.A., Napi, N.N.L.M., Mansor, W.N.W., Ahmed, A.N., Ismail, M., Ramly, Z.T.A., 2020. Air quality status during 2020 Malaysia Movement Control Order (MCO) due to 2019 novel coronavirus (2019-nCoV) pandemic. *Sci. Total Environ.* 729, 139022. <https://doi.org/10.1016/j.scitotenv.2020.139022>.
- Air Quality e-Reporting, 2020. The European Air Quality Database. European Environment Agency. <https://www.eea.europa.eu/data-and-maps/data/aqereporting-8>. (Accessed 1 March 2021).
- Apple, 2020. Mobility Trends Reports. <https://covid19.apple.com/mobility>. (Accessed 1 March 2021).
- Barré, J., Petetin, H., Colette, A., Guevara, M., Peuch, V.-H., Rouil, L., Engelen, R., Inness, A., Flemming, J., Pérez García-Pando, C., Bowdalo, D., Meleux, F., Geels, C., Christensen, J.H., Gauss, M., Benedictow, A., Tsyro, S., Frieze, E., Struzewska, J., Kaminski, J.W., Douros, J., Timmermans, R., Robertson, L., Adani, M., Jorba, O., Joly, M., Kouznetsov, R., 2020. Estimating lockdown induced European NO₂ changes. *Atmos. Chem. Phys. Discuss.* <https://doi.org/10.5194/acp-2020-995> in review.
- Bechle, M.J., Millet, D.B., Marshall, J.D., 2015. National spatiotemporal exposure surface for NO₂: monthly scaling of a satellite-derived land-use regression, 2000–2010. *Environ. Sci. Technol.* 49 (20), 12297–12305. <https://doi.org/10.1021/acs.est.5b02882>.
- Belocconi, A., Vounatsou, P., 2020. Bayesian geostatistical modelling of high-resolution NO₂ exposure in Europe combining data from monitors, satellites and chemical transport models. *Environ. Int.* 138, 105578. <https://doi.org/10.1016/j.envint.2020.105578>.
- Belocconi, A., Kamarianakis, Y., Chrysoulakis, N., 2016. Estimating urban PM₁₀ and PM_{2.5} concentrations, based on synergistic MERIS/AATSR aerosol observations, land cover and morphology data. *Remote Sens. Environ.* 172, 148–164. <https://doi.org/10.1016/j.rse.2015.10.017>.
- Belocconi, A., Chrysoulakis, N., Lyapustin, A., Utzinger, J., Vounatsou, P., 2018. Bayesian geostatistical modelling of PM₁₀ and PM_{2.5} surface level concentrations in Europe using high-resolution satellite-derived products. *Environ. Int.* 121, 57–70. <https://doi.org/10.1016/j.envint.2018.08.041>.
- Benas, N., Belocconi, A., Chrysoulakis, N., 2013. Estimation of urban PM₁₀ concentration, based on MODIS and MERIS/AATSR synergistic observations. *Atmos. Environ.* 79, 448–454. <https://doi.org/10.1016/j.atmosenv.2013.07.012>.
- Blangiardo, M., Cameletti, M., 2015. Spatial and Spatio-temporal Bayesian Models With R - INLA. <https://doi.org/10.1002/9781118950203>.
- Brauer, M., Freedman, G., Frostad, J., Van Donkelaar, A., Martin, R.V., Dentener, F., Dingenen, R.V., Estep, K., Amini, H., Apte, J.S., Balakrishnan, K., Barregard, L., Broday, D., Feigin, V., Ghosh, S., Hopke, P.K., Knibbs, L.D., Kokubo, Y., Liu, Y., Ma, S., Morawska, L., Sangrador, J.L.T., Shaddick, G., Anderson, H.R., Vos, T., Forouzanfar, M.H., Burnett, R.T., Cohen, A., 2016. Ambient air pollution exposure estimation for the global burden of disease 2013. *Environ. Sci. Technol.* 50 (1), 79–88. <https://doi.org/10.1021/acs.est.5b03709>.
- Brunekreef, B., Downward, G., Forastiere, F., Gehring, U., Heederik, D.J.J., Hoek, G., Koopmans, M.P.G., Smit, L.A.M., Vermeulen, R.C.H., 2021. Air pollution and COVID-19. Including elements of air pollution in rural areas, indoor air pollution and vulnerability and resilience aspects of our society against respiratory disease, social inequality stemming from air pollution. Study for the Committee on Environment, Public Health and Food Safety, Policy Department for Economic, Scientific and Quality of Life Policies, European Parliament, Luxembourg [https://www.europarl.europa.eu/RegData/etudes/STUD/2021/658216/IPOL_STU\(2021\)658216_EN.pdf](https://www.europarl.europa.eu/RegData/etudes/STUD/2021/658216/IPOL_STU(2021)658216_EN.pdf). (Accessed 1 March 2021).
- Chen, J.C., Schwartz, J., 2008. Metabolic syndrome and inflammatory responses to long-term particulate air pollutants. *Environ. Health Perspect.* 116 (5), 612–617. <https://doi.org/10.1289/ehp.10565>.
- Chudnovsky, A.A., Koutrakis, P., Kloog, I., Melly, S., Nordio, F., Lyapustin, A., Wang, Y., Schwartz, J., 2014. Fine particulate matter predictions using high resolution Aerosol Optical Depth (AOD) retrievals. *Atmos. Environ.* 89, 189–198. <https://doi.org/10.1016/j.atmosenv.2014.02.019>.
- Cohen, A.J., Brauer, M., Burnett, R., Anderson, H.R., Frostad, J., Estep, K., Balakrishnan, K., Brunekreef, B., Dandona, L., Dandona, R., Feigin, V., Freedman, G., Hubbell, B., Jobling, A., Kan, H., Knibbs, L., Liu, Y., Martin, R., Morawska, L., Pope III, C.A., Shin, H., Straif, K., Shaddick, G., Thomas, M., van Dingenen, R., van Donkelaar, A., Vos, T., Murray, C.J.L., Forouzanfar, M.H., 2017. Estimates and 25-year trends of the global burden of disease attributable to ambient air pollution: an analysis of data from the Global Burden of Diseases Study 2015. *Lancet* 389 (10082), 1907–1918. [https://doi.org/10.1016/S0140-6736\(17\)30505-6](https://doi.org/10.1016/S0140-6736(17)30505-6).
- Copernicus Atmosphere Monitoring Service (CAMS), 2020a. Regional Air Quality. <http://www.regional.atmosphere.copernicus.eu>. (Accessed 1 March 2021).
- Copernicus Atmosphere Monitoring Service (CAMS), 2020b. Regional Air Quality. COVID impact on air quality in Europe. A preliminary regional model analysis. https://policy.atmosphere.copernicus.eu/reports/CAMS71_COVID_20200626_v1.3.pdf. (Accessed 1 March 2021).
- Copernicus Land Monitoring Services (CLMS), 2020. Pan-European data products. <http://land.copernicus.eu/pan-european>. (Accessed 1 March 2021).
- CORINE Land Cover, 2012. Copernicus Land Monitoring Services. <http://land.copernicus.eu/pan-european/corine-land-cover/clc-2012/>. (Accessed 1 March 2021).
- Dantas, G., Siciliano, B., França, B.B., da Silva, C.M., Arbilla, G., 2020. The impact of COVID-19 partial lockdown on the air quality of the city of Rio de Janeiro, Brazil. *Sci. Total Environ.* 729, 139085. <https://doi.org/10.1016/j.scitotenv.2020.139085>.
- Digital Elevation Model Over Europe (EU-DEM). European Environment Agency <http://www.eea.europa.eu/data-and-maps/data/eu-dem>. (Accessed 1 March 2021).
- Dobson, R., Semple, S., 2020. Changes in outdoor air pollution due to COVID-19 lockdowns differ by pollutant: evidence from Scotland. *Occup. Environ. Med.* 77 (11), 798–800. <https://doi.org/10.1136/oemed-2020-106659>.
- Europe Coastline Shapefile. European Environment Agency <http://www.eea.europa.eu/data-and-maps/data/eea-coastline-for-analysis-1/gis-data/europe-coastline-shapefile>. (Accessed 1 March 2021).
- European Environment Agency (EEA), 2016. Air quality in Europe – 2016 report. EEA Report No. 28/2016.
- European Settlement Map, 2016. Copernicus Land Monitoring Services, Related Pan-European Products. <https://land.copernicus.eu/pan-european/GHSL/european-settlement-map>. (Accessed 1 March 2021).
- Gelfand, A.E., Kim, H.-J., Sirmans, C.F., Banerjee, S., 2003. Spatial modeling with spatially varying coefficient processes. *J. Am. Stat. Assoc.* 98 (462), 387–396. <https://doi.org/10.1198/016214503000170>.
- Gelman, A., Hwang, J., Vehtari, A., 2014. Understanding predictive information criteria for Bayesian models. *Stat. Comput.* 24 (6), 997–1016. <https://doi.org/10.1007/s11222-013-9416-2>.
- Giani, P., Castruccio, S., Anav, A., Howard, D., Hu, W., Crippa, P., 2020. Short-term and long-term health impacts of air pollution reductions from COVID-19 lockdowns in China and Europe: a modelling study. *Lancet Planet. Health* 4 (10), E474–E482. [https://doi.org/10.1016/s2542-5196\(20\)30224-2](https://doi.org/10.1016/s2542-5196(20)30224-2).
- Goldberg, D.L., Anenberg, S.C., Griffin, D., McLinden, C.A., Lu, Z., Streets, D.G., 2020. Disentangling the impact of the COVID-19 lockdowns on urban NO₂ from natural variability. *Geophys. Res. Lett.* 47 (17). <https://doi.org/10.1029/2020GL089269>.
- Google Earth Engine Team, 2015. Google Earth Engine: A Planetary-scale Geospatial Analysis Platform. <https://earthengine.google.com>. (Accessed 1 March 2021).
- Guevara, M., Jorba, O., Soret, A., Petetin, H., Bowdalo, D., Serradell, K., Tena, C., Denier van der Gon, H., Kuenen, J., Peuch, V.-H., Pérez García-Pando, C., 2020. Time-resolved emission reductions for atmospheric chemistry modelling in Europe during the COVID-19 lockdowns. *Atmos. Chem. Phys. Discuss.* <https://doi.org/10.5194/acp-2020-686> in review.
- He, Q., Huang, B., 2018. Satellite-based mapping of daily high-resolution ground PM_{2.5} in china via space-time regression modeling. *Remote Sens. Environ.* 206, 72–83. <https://doi.org/10.1016/j.rse.2017.12.018>.
- Huang, L., Liu, Z., Li, H., Wang, Y., Li, Y., Zhu, Y., ... Li, L., 2020. The silver lining of COVID-19: estimation of short-term health impacts due to lockdown in the Yangtze River Delta region, China. *Geohealth* <https://doi.org/10.1029/2020GH000272>.
- Imperviousness Degree, 2015. Copernicus Land Monitoring Services, High Resolution Layers. <https://land.copernicus.eu/pan-european/high-resolution-layers/imperviousness/status-maps/2015>. (Accessed 1 March 2021).
- Inness, A., Aedes, M., Agustí-Panareda, A., Barr, J., Benedictow, A., Blechschmidt, A., Jose Dominguez, J., Engelen, R., Eskes, H., Flemming, J., Huijnen, V., Jones, L., Kipling, Z., Massart, S., Parrington, M., Peuch, V., Razinger, M., Remy, S., Schulz, M., Suttie, M., 2019. The CAMS reanalysis of atmospheric composition. *Atmos. Chem. Phys.* 19 (6), 3515–3556. <https://doi.org/10.5065/D61C1TXF>.
- Larkin, A., Geddes, J.A., Martin, R.V., Xiao, Q., Liu, Y., Marshall, J.D., Brauer, M., Hystad, P., 2017. Global land use regression model for nitrogen dioxide air pollution. *Environ. Sci. Technol.* 51 (12), 6957–6964. <https://doi.org/10.1021/acs.est.7b01148>.
- Lindgren, F., Rue, H., Lindström, J., 2011. An explicit link between Gaussian fields and Gaussian Markov random fields: the stochastic partial differential equation approach. *J. R. Stat. Soc. Ser. B Stat Methodol.* 73 (4), 423–498. <https://doi.org/10.1111/j.1467-9868.2011.00777.x>.
- Liu, F., Page, A., Strode, S.A., Yoshida, Y., Choi, S., Zheng, B., Lamsal, L.N., Li, C., Krotkov, N.A., Eskes, H., van der Ronald, A., Veeffkind, P., Levelt, P.F., Hauser, O.P., Joiner, J., 2020. Abrupt decline in tropospheric nitrogen dioxide over china after the outbreak of COVID-19. *Sci. Adv.* 6 (28). <https://doi.org/10.1126/sciadv.abc2992>.
- Menuet, L., Bessagnet, B., Siour, G., Mailler, S., Pennel, R., Cholokian, A., 2020. Impact of lockdown measures to combat COVID-19 on air quality over western Europe. *Sci. Total Environ.* 741, 140426. <https://doi.org/10.1016/j.scitotenv.2020.140426>.
- Mostafavi, N., Jeong, A., Vlaanderen, J., Imboden, M., Vineis, P., Jarvis, D., Kogevinas, M., Probst-Hensch, N., Vermeulen, R., 2019. The mediating effect of immune markers on the association between ambient air pollution and adult-onset asthma. *Sci. Rep.* 9 (1), 8818. <https://doi.org/10.1038/s41598-019-45327-4>.
- Nighttime Lights, 2013. NOAA's National Geophysical Data Center. DMS-OLS Nighttime Lights Time Series Version 4. <https://www.ngdc.noaa.gov/eog/dmsp/downloadV4composites.html>. (Accessed 1 March 2021).
- Normalized Difference Vegetation Index (NDVI) Daily, 2020. Google, MODIS Aqua and Terra. https://developers.google.com/earth-engine/datasets/catalog/MODIS_MOD09GA_006_NDVI. (Accessed 1 March 2021).
- Novotny, E.V., Bechle, M.J., Millet, D.B., Marshall, J.D., 2011. National satellite-based land-use regression: NO₂ in the United States. *Environ. Sci. Technol.* 45 (10), 4407–4414. <https://doi.org/10.1021/es103578x>.
- Ntzoufras, I., 2008. Bayesian Modeling Using WinBUGS. <https://doi.org/10.1002/9780470434567>.

- OECD (Organisation for Economic Co-operation and Development), 2020. OECD Economic Outlook, Volume 2020 Issue 2. OECD Publishing, Paris <https://doi.org/10.1787/39a88ab1-en>.
- Ogen, Y., 2020. Assessing nitrogen dioxide (NO₂) levels as a contributing factor to coronavirus (COVID-19) fatality. *Sci. Total Environ.* 726, 138605. <https://doi.org/10.1016/j.scitotenv.2020.138605>.
- Powers, J.G., Klemp, J.B., Skamarock, W.C., Davis, C.A., Dudhia, J., Gill, D.O., Coen, J.L., Gochis, D.J., Ahmadov, R., Peckham, S.E., Grell, G.A., Michalakes, J., Trahan, S., Benjamin, S.G., Alexander, C.R., Dimigo, G.J., Wang, W., Schwartz, C.S., Romine, G.S., Liu, Z., Snyder, C., Chen, F., Barlage, M.J., Yu, W., Duda, M.G., 2017. The weather research and forecasting model: overview, system efforts, and future directions. *Bull. Am. Meteorol. Soc.* 98 (8), 1717–1737 (2016). <https://doi.org/10.1175/BAMS-D-15-00308.1>.
- Putaud, J.P., Pozzoli, L., Pisoni, E., Martins Dos Santos, S., Lagler, F., Lanzani, G., Dal Santo, U., Colette, A., 2020. Impacts of the COVID-19 lockdown on air pollution at regional and urban background sites in northern Italy. *Atmos. Chem. Phys.* <https://doi.org/10.5194/acp-2020-755> in review.
- R Core Team, 2015. R: A Language and Environment for Statistical Computing. R Foundation for Statistical Computing, Vienna, Austria <http://www.R-project.org/>. (Accessed 1 March 2021).
- Rue, H., Martino, S., Chopin, N., 2009. Approximate Bayesian inference for latent Gaussian models by using integrated nested Laplace approximations. *J. R. Stat. Soc. Ser. B Stat Methodol.* 71 (2), 319–392. <https://doi.org/10.1111/j.1467-9868.2008.00700.x>.
- Rue, H., Martino, S., Lindgren, F., Simpson, D., Riebler, A., 2013. R-INLA: Approximate Bayesian Inference Using Integrated Nested Laplace Approximations. Trondheim, Norway. <http://www.r-inla.org>. (Accessed 1 March 2021).
- Saha, S., Moorthi, S., Wu, X., Wang, J., Nadiga, S., Tripp, P., Behringer, D., Hou, Y., Chuang, H., Iredell, M., Ek, M., Meng, J., Yang, R., Mendez, M.P., van den Dool, H., Zhang, Q., Wang, W., Chen, M., Becker, E., 2011. NCEP Climate Forecast System Version 2 (CFSv2) 6-hourly Products, Research Data Archive at the National Center for Atmospheric Research, Computational and Information Systems Laboratory. <https://doi.org/10.5065/D61C1TXF>. (Accessed 1 March 2021).
- Shakil, M.H., Munim, Z.H., Tasnia, M., Sarowar, S., 2020. COVID-19 and the environment: a critical review and research agenda. *Sci. Total Environ.* 745, 141022. <https://doi.org/10.1016/j.scitotenv.2020.141022>.
- Sharma, S., Zhang, M., Anshika, Gao, J., Zhang, H., Kota, S.H., 2020. Effect of restricted emissions during COVID-19 on air quality in India. *Sci. Total Environ.* 728, 138878. <https://doi.org/10.1016/j.scitotenv.2020.138878>.
- Shi, Z., Song, C., Liu, B., Lu, G., Xu, J., Van Vu, T., ... Harrison, R.M., 2021. Abrupt but smaller than expected changes in surface air quality attributable to COVID-19 lockdowns. *Sci. Adv.* 7 (3). <https://doi.org/10.1126/sciadv.abd6696> eabd6696.
- Spiegelhalter, D.J., Best, N.G., Carlin, B.P., Van Der Linde, A., 2002. Bayesian measures of model complexity and fit. *J. R. Stat. Soc. Ser. B Stat Methodol.* 64 (4), 583–616. <https://doi.org/10.1111/1467-9868.00353>.
- Stafoggia, M., Schwartz, J., Badaloni, C., Bellander, T., Alessandrini, E., Cattani, G., de Donato, F., Gaeta, A., Leone, G., Lyapustin, A., Sorek-Hamer, M., de Hoogh, K., Di, Q., Forastiere, F., Kloog, I., 2017. Estimation of daily PM₁₀ concentrations in Italy (2006–2012) using finely resolved satellite data, land use variables and meteorology. *Environ. Int.* 99, 234–244. <https://doi.org/10.1016/j.envint.2016.11.024>.
- Tree Cover Density, 2015. Copernicus Land Monitoring Services, High Resolution Layers. <https://land.copernicus.eu/pan-european/high-resolution-layers/forests/tree-cover-density/status-maps/2015>. (Accessed 1 March 2021).
- Veefkind, J.P., Aben, I., McMullan, K., Förster, H., De Vries, J., Otter, G., ... Van Weele, M., 2012. TROPOMI on the ESA Sentinel-5 Precursor: a GMES mission for global observations of the atmospheric composition for climate, air quality and ozone layer applications. *Remote Sens. Environ.* 120 (70–83), 2012. <https://doi.org/10.1016/j.rse.2011.09.027>.
- Venter, Z.S., Aunan, K., Chowdhury, S., Lelieveld, J., 2020. COVID-19 lockdowns cause global air pollution declines. *Proc. Natl. Acad. Sci. U. S. A.* 117 (32), 18984–18990. <https://doi.org/10.1073/pnas.2006853117>.
- Wang, B., Li, R., Lu, Z., Huang, Y., 2020. Does comorbidity increase the risk of patients with covid-19: Evidence from meta-analysis. *Aging* 12 (7), 6049–6057. <https://doi.org/10.18632/AGING.103000>.
- Watanabe, S., 2013. A widely applicable Bayesian information criterion. *J. Mach. Learn. Res.* 14 (1), 867–897.
- Xiang, J., Austin, E., Gould, T., Larson, T., Shirai, J., Liu, Y., Marshall, J., Seto, E., 2020. Impacts of the COVID-19 responses on traffic-related air pollution in a Northwestern US city. *Sci. Total Environ.* 747, 141325. <https://doi.org/10.1016/j.scitotenv.2020.141325>.
- Yang, J., Zheng, Y., Gou, X., Pu, K., Chen, Z., Guo, Q., Ji, R., Wang, H., Wang, Y., Zhou, Y., 2020. Prevalence of comorbidities and its effects in coronavirus disease 2019 patients: a systematic review and meta-analysis. *Int. J. Infect. Dis.* 94, 91–95. <https://doi.org/10.1016/j.ijid.2020.03.017>.
- Young, M.T., Bechle, M.J., Sampson, P.D., Szpiro, A.A., Marshall, J.D., Sheppard, L., Kaufman, J.D., 2016. Satellite-based NO₂ and model validation in a national prediction model based on universal kriging and land-use regression. *Environ. Sci. Technol.* 50 (7), 3686–3694. <https://doi.org/10.1021/acs.est.5b05099>.
- Zhang, R., Zhang, Y., Lin, H., Feng, X., Fu, T.M., Wang, Y., 2020. NO_x emission reduction and recovery during COVID-19 in East China. *Atmosphere* 11 (4), 433. <https://doi.org/10.3390/ATMOS11040433>.